Favorable Conditions for Magnetic Reconnection at Ganymede's Upstream Magnetopause

N. Kaweeyanun[1] [iD], **A. Masters[1]** [iD], and **X. Jia[2]** [iD]

[1]Department of Physics, Imperial College London, London, UK, [2]Department of Climate and Space Sciences and Engineering, University of Michigan, Ann Arbor, MI, USA

Abstract Ganymede is the only Solar System moon known to generate a permanent magnetic field. Jovian plasma motions around Ganymede create an upstream magnetopause, where energy flows are thought to be driven by magnetic reconnection. Simulations indicate Ganymedean reconnection events may be transient, but the nature of magnetopause reconnection at Ganymede remains poorly understood, requiring an assessment of reconnection onset theory. We present an analytical model of steady-state conditions at Ganymede's magnetopause, from which the first Ganymedean reconnection onset assessment is conducted. We find that reconnection may occur wherever Ganymede's closed magnetic field encounters Jupiter's ambient magnetic field, regardless of variations in magnetopause conditions. Unrestricted reconnection onset highlights possibilities for multiple X lines or widespread transient reconnection at Ganymede. The reconnection rate is controlled by the ambient Jovian field orientation and hence driven by Jupiter's rotation. Future progress on this topic is highly relevant for the JUpiter ICy moon Explorer mission.

Plain Language Summary Ganymede is the largest moon of Jupiter and the only Solar System moon that produces its own magnetic field. Ganymede's magnetic field is surrounded by Jupiter's much larger magnetic field, which flows around the moon like a river flowing around a rock. The boundary where Jupiter's magnetic field first encounters Ganymede's is called the magnetopause. At this boundary, energy and mass can move between the two magnetic fields through a process called magnetic reconnection. Our paper introduces a simple model of Ganymede's magnetopause and uses this model to show where reconnection can occur on the boundary. We find that reconnection can occur anywhere on the magnetopause for any plausible environmental conditions around Ganymede, so the locations where these energy-releasing events occur may be particularly unpredictable. The rate of energy released by reconnection meanwhile depends on near-Ganymede conditions, which change significantly as Jupiter rotates. These results will help inform the planning of the JUpiter ICy moon Explorer mission to Ganymede.

1. Introduction

Ganymede (radius R_G = 2,634 km) is the largest moon of Jupiter (equatorial radius R_J = 71,492 km) and the Solar System. Ganymede uniquely generates a permanent magnetic field as discovered by measurements from both the magnetometer (Kivelson et al., 1996; Kivelson et al., 1997) and the plasma wave subsystem aboard the Galileo spacecraft (Gurnett et al., 1996). The permanent magnetic field is likely dipolar and produced by dynamo action within Ganymede's molten iron core (Anderson et al., 1996; Schubert et al., 1996). The equatorial surface dipole strength is 719 nT, approximately seven times stronger than the ambient Jovian magnetic field, and the dipole axis typically tilts ~176° from Ganymede's spin axis (Kivelson et al., 2002). The dipole axis orientation varied over the short time scales between Galileo flybys, thought to be very likely due to an additional, induced magnetic field arising from electromagnetic induction in a subsurface ocean (Kivelson et al., 2002). Obtaining detailed knowledge of this potentially life-sustaining water source is the primary objective for the upcoming JUpiter ICy moon Explorer (JUICE) mission (Grasset et al., 2013).

Ganymede orbits Jupiter at an average distance of ~15 R_J in a plane nearly coplanar to Jupiter's spin equator (Bills, 2005; McKinnon, 1997). The orbital plane is ~7° inclined with respect to the central plane of a ~3 R_J thick, rotating Jovian magnetospheric plasma sheet arising from Io's volcanic activity (Kivelson et al., 2004). Ganymede thus effectively moves up and down through the plasma sheet, experiencing large variations in

the ambient plasma and magnetic conditions. Inside the plasma sheet, there also exists a thin current sheet approximately coplanar to the plasma sheet's central plane (e.g., Cowley et al., 2003). Hence, the ambient Jovian magnetized plasma conditions at Ganymede are controlled by the distance between Ganymede and the center of Jupiter's current sheet.

The Jovian plasma rotates with the planet at ~80% of the corotation speed at Ganymede (Williams, Mauk, & McEntire, 1997; Williams, Mauk, McEntire, & Roelof, et al., 1997), which is much faster than Ganymede's Keplerian speed. Hence, the magnetic field frozen into the plasma compresses Ganymede's magnetic field on the upstream side forming a magnetopause boundary (Jia et al., 2008). The Jovian plasma flow is sub-Alfvénic so the magnetic pressure predominantly shapes magnetopause interactions (Neubauer, 1998). Consequently, Ganymede's magnetosphere is cylindrically shaped with long Alfvén wings and no bow shock preceding the magnetopause (Jia et al., 2010)— a contrast to planetary magnetospheres, which are bullet-shaped due to dynamic pressure dominance in the super-Alfvénic solar wind (Neubauer, 1990). Magnetic field lines near the upstream equator inside the magnetosphere are closed (both ends at Ganymede's magnetic poles) and almost antiparallel (due to 176° dipole tilt) to Jupiter's magnetic field lines, which hints at magnetic reconnection as the dominant mechanism for plasma and energy inflows from Jupiter to Ganymede. Elsewhere, magnetic field lines in Ganymede's large polar caps and magnetotail are open (at least one end at Jupiter), allowing particles entries/escapes from the moon's magnetosphere (Frank et al., 1997; Williams, Mauk, & McEntire, 1997; Williams, Mauk, McEntire, Roelof, et al., 1997).

The Ganymedean magnetosphere has been modeled by many numerical simulations, some of which discuss magnetic reconnection at the upstream magnetopause. For instance, Jia et al. (2008, 2009) produced a global three-dimensional resistive magnetohydrodynamic (MHD) simulation of Ganymede that showed transient reconnection signatures spread over large regions of the magnetopause. Subsequent analysis revealed these signals to be consistent with intermittent rope-like flux-transfer events (Jia et al., 2010). Recently, modeling work has been extended to include the Hall effect (Dorelli et al., 2015) and to couple with kinetic-ion hybrid (Leclercq et al., 2016) and local particle-in-cell codes (Daldorff et al., 2014; Tóth et al., 2016; Zhou et al., 2019), all of which treat reconnection microphysics more directly. Specifically, the MHD-EPIC (embedded particle-in-cell) model indicated presence of quasiperiodic formation of flux-transfer events consistent with previous resistive-MHD results and Galileo observations. However, these comprehensive numerical modeling studies have not been supported by important assessment of reconnection at Ganymede's magnetopause that apply reconnection onset theory, which is an essential additional element in understanding the physics at work.

We have used an analytical approach to parametrize the magnetopause conditions expected from a typical Jovian plasma flow around Ganymede. This approach provides a computationally cheap way to apply modern kinetic physics of reconnection onset that is challenging to implement in more expensive numerical models. Reconnection onset has been analytically assessed at Earth (Alexeev et al., 1998; Trattner et al., 2007a, 2007b), Jupiter (Desroche et al., 2012; Masters, 2017), Saturn (Desroche et al., 2013; Masters, 2015a), Uranus (Masters, 2014), and Neptune (Masters, 2015b). In the following sections, we outline the analytical model of Ganymede's upstream magnetopause followed by the first kinetic assessment of magnetic reconnection onset and structural properties.

2. Analytical Model of Ganymede's Upstream Magnetopause

Maps of conditions immediately either side of Ganymede's magnetopause are essential for reconnection onset assessment. To achieve this, we must first define the magnetopause surface. Kivelson et al. (1998) describe Ganymede's magnetosphere as a cylinder with shifting center points in dynamical Ganymede-at-origin Jovian magnetic field-aligned coordinates (GphiB). We rewrite the equations for Ganymede's magnetopause surface in Ganymede-at-origin Cartesian coordinates (GphiO) in which X points along the plasma flow direction, Y points from Ganymede to Jupiter, and Z points along Jupiter's spin axis (approximately parallel to Ganymede's spin axis due to small Ganymedean orbit inclination) as follows:

$$f(X, Y, Z) = \frac{(X - X_0)^2}{a^2} + \frac{(Y \cos\theta_r - Z \sin\theta_r - Y_0)^2}{b^2} = 1,$$
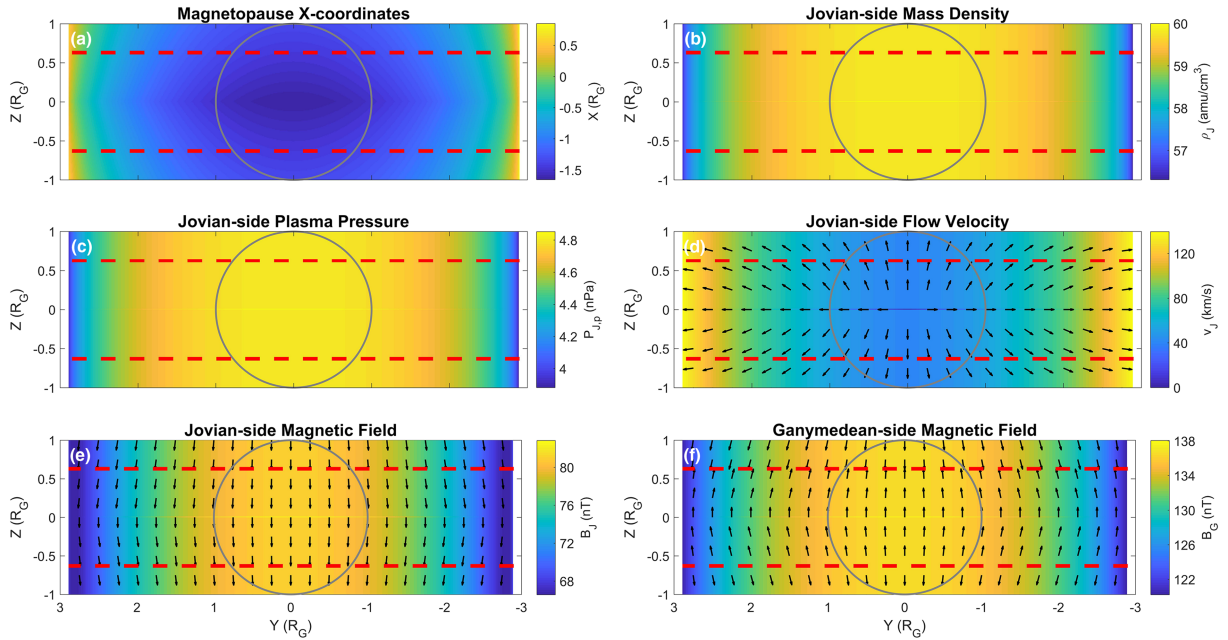
where

Figure 1. Magnetopause conditions projected onto a two-dimensional plane with the Jovian plasma flowing into the page when Ganymede is in the Jovian current sheet. Parameters shown are (a) X coordinates on the magnetopause surface, (b) Jovian-side mass density, (c) Jovian-side plasma pressure, (d) Jovian-side flow velocity, (e) Jovian-side magnetic field, and (f) Ganymedean-side magnetic field. Ganymede is outlined in gray, and the closed-field region is defined between two red dashed lines.

$$\theta_r = tan^{-1}\left(\frac{|B_{0,z}|}{B_{0,y}}\right) - 90°,$$

$$X_0(Y,Z) = X_0(0) + |Ysin\theta_r + Zcos\theta_r|tan\theta,$$

$$Y_0(Y,Z) = \frac{2}{\pi}Y_{0.max}sin(\phi - 248°)tan^{-1}\left(\frac{Ysin\theta_r + Zcos\theta_r}{\lambda}\right).$$

The angle θ_r describes right-handed rotation angle between GphiB and GphiO coordinates. $(B_{0,y}, B_{0,z})$ are the ambient Jovian magnetic field components. (X_0, Y_0) denote the center point offsets from the GphiO origin. Kivelson et al. (1998) chose $a = 2.2\,R_G$ and $\lambda = 0.5\,R_G$ and then used a least squares fit to the Galileo data to calculate $b = 2.90\,R_G$, $X_0(0) = 0.544\,R_G$, $Y_{0,max} = 0.914\,R_G$, and $\theta = 0.298$ radians. This leaves Jupiter's System III east longitude ϕ as the only free parameter. System III coordinates describe a stationary Jovian magnetic dipole with Ganymede orbiting quickly through the longitudes, which is equivalent to a rapidly spinning dipole in Ganymede-stationary GphiO coordinates. As the Jovian plasma/current sheets move with the dipole, each ϕ value determines their positions relative to Ganymede, and thus ambient plasma/magnetic conditions that control reconnection.

From these equations we can generate Ganymede's upstream ($X < 0\,R_G$) magnetopause grid surface between $-4.0\,R_G < Y < 4.0\,R_G$ and $-1.0\,R_G < Z < 1.0\,R_G$ with $0.01\,R_G$ resolution in both dimensions. The magnetopause is projected onto a Y-Z plane as shown in Figure 1a when Ganymede is in the Jovian current sheet ($\phi = 248°$). Here the magnetopause is north–south symmetric with the standoff distance of $1.65\,R_G$ calculated at the subflow point ($Y = 0\,R_G$, $Z = 0\,R_G$). The magnetopause X coordinate increases away from the subflow point in all directions as the surface curves downstream. The magnetopause gains maximum north-south asymmetries when Ganymede is furthest above/below the current sheet ($\phi = 158°, 338°$). These asymmetries occur in response to changes in ambient Jovian magnetic field orientations (parametrizations below). This simple and fixed magnetopause description is sufficient for reconnection onset assessment, as more accurate surface models will not affect the conclusions drawn.

Next, we describe the Jovian-side (external) conditions at the magnetopause. The ambient Jovian plasma mass density is $\rho_0 = 56$ amu/cm^3 when Ganymede is in the current sheet and $\rho_0 = 28$ amu/cm^3 when

Ganymede is furthest above/below the current sheet (Jia et al., 2008). The plasma is compressed near Ganymede's magnetopause, thus increasing its mass density. We employ a simple compression formula $\rho_J = A_1 \cos(\alpha) + \rho_0$, where α is the flaring angle between the X axis and the local magnetopause-normal vector. The cosine of flaring angle is adapted from results at Earth's magnetopause (Petrinec & Russell, 1997) and captures spatial density variations expected from plasma flows around a cylindrical magnetosphere. A more complex compression description is again possible but unlikely to affect main conclusions drawn. The typical compression amplitude $A_1 = 4$ amu/cm^3 is estimated empirically from numerical simulations (Jia et al., 2008; Tóth et al., 2016), and the added ambient mass density ρ_0 prevents plasma decompression. Figure 1b shows the Jovian-side mass density variation when Ganymede is in the current sheet. The density peaks near the subflow point where Jovian plasma collides head-on with the magnetopause and decreases toward the flanks where plasma flows near parallel to the surface.

The ambient Jovian plasma pressure (thermal and energetic) is $P_0 = 3.8$ nPa when Ganymede is in the current sheet and $P_0 = 1.9$ nPa when Ganymede is furthest above/below the current sheet (Jia et al., 2008; Kivelson et al., 2004). Figure 1c shows plasma pressure at the Jovian-side magnetopause when Ganymede is in the current sheet. Like mass density, a cosine relation $P_{J,p} = A_2 \cos(\alpha) + P_0$ parametrizes the pressure compression. The amplitude $A_2 = 1.05$ nPa is approximated from the pressure relation at Earth's magnetopause for slow plasma flow speeds (Petrinec & Russell, 1997). This method provides slightly smaller Jovian-side plasma pressures (~1 nPa difference) compared to numerically simulated values. However, larger pressures are found to cause unrealistic Jovian magnetic field decompression at the magnetopause (discussed below).

The ambient Jovian plasma flows along the X axis at speed $v_0 = 140$ km/s in Ganymede's rest frame (Jia et al., 2008). Figure 1d shows the plasma flow velocity at the Jovian-side magnetopause when Ganymede is in the current sheet. Unlike mass density and pressure, we parametrize the flow speed by a sine relation $v_J = v_0 \sin(\alpha)$ as the ambient plasma is most stagnated by direct collision near the subflow point. The Jovian-side flow directions (normalized arrows) are constrained to be parallel to the magnetopause surface and orthogonal to cross products of magnetopause-normal vectors and ambient plasma flow vectors.

The ambient Jovian magnetic field has been computed at Ganymede using a mathematical model (Jia et al., 2008; Khurana, 1997). The magnetic field strength has minima of $B_0 \sim 70$ nT when Ganymede is in the current sheet and maxima of $B_0 \sim 105$ nT when Ganymede is furthest above/below the current sheet. Following Jia et al. (2008), we assume negligible x component $B_{0,x}$ and parametrize the remaining two components by $B_{0,y} = 84\sin(\phi - 248°)$ nT and $B_{0,z} = 3\cos(\phi) - 79$ nT. Hence, the ambient Jovian magnetic field always points southward in the Y-Z plane between 135° and 225° clock angles. We quantify magnetic field compression at the Jovian-side magnetopause using conservation of combined magnetic, plasma, and dynamic pressures before and after the compression. The total precompression pressure can be calculated from ambient plasma/magnetic values. Using data from Figures 1c and 1d, we derive postcompression plasma pressure and magnetopause-parallel dynamic pressure component. We subtract these values from the total pressure to obtain the postcompression magnetic pressure $P_{J,b}$ (which includes the magnetopause-normal dynamic pressure component) and convert this into Jovian-side magnetic field strength B_J shown in Figure 1e when Ganymede is in the current sheet. The plasma compression also constrains magnetic field directions (normalized arrows) onto the magnetopause surface.

The Jovian-side plasma and magnetic pressures together exert force on Ganymede's magnetopause, which is balanced by magnetic pressure from Ganymede's magnetic field given negligible plasma pressure inside the moon's magnetosphere (Jia et al., 2008). Hence, we can derive the magnetic field strength at the Ganymedean-side magnetopause B_G as shown in Figure 1f when Ganymede is in the current sheet. Magnetic field directions (normalized arrows) have no azimuthal component (consistent with dipolar field) and lie parallel to the magnetopause surface. The magnetic field points northward in the "closed-field region" defined by $|Z| < 0.63$ R$_G$ and southward elsewhere (Jia et al., 2009). The closed-field region is bounded by two horizontal red dashed lines, which we retroactively add to all Figure 1 subplots. Otherwise, the Ganymedean-side plasma density and flow speed are set to uniform values $\rho_G = 20$ amu/cm^3 (Jia et al., 2008, 2009) and $v_G = 0$ km/s (approximating relatively slow plasma flows inside Ganymede's magnetosphere), respectively.
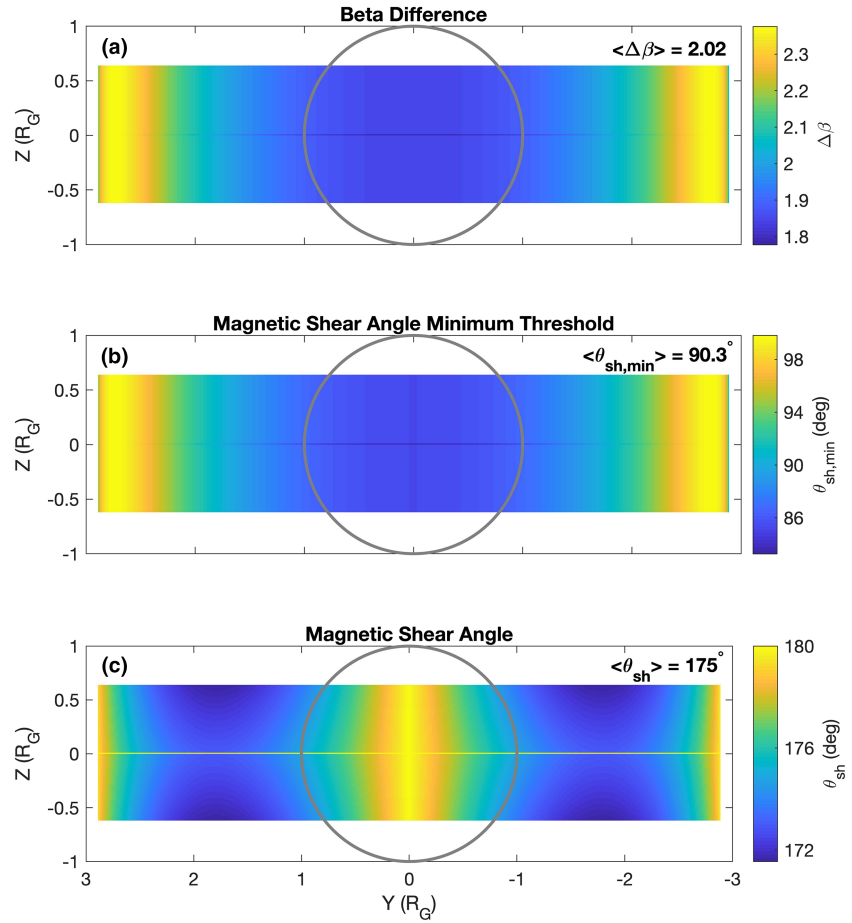
Figure 2. Evaluation of the diamagnetic drift onset condition in Ganymede's closed-field region when Ganymede is in the Jovian current sheet. Parameters shown are (a) beta difference across the magnetopause, (b) magnetic shear angle minimum threshold, and (c) magnetic shear angle calculated from magnetopause conditions. Ganymede is outlined in gray, and average parameter values are shown at top right.

3. Magnetic Reconnection Assessment at Ganymede

With maps of conditions on both sides of Ganymede's magnetopause, we can assess reconnection onset specifically for the closed-field region where particle transport is not expected under MHD theory. Reconnection onset requires three conditions to be satisfied. First, the magnetopause current sheet separating Jupiter's and Ganymede's magnetic fields must be thinner than approximately an ion inertial length to break the MHD frozen-in flux condition (Phan et al., 2011). The Galileo data analysis revealed the magnetopause current sheet thickness to be <400 km (Kivelson et al., 1998), similar to the ~426 km ion inertial length calculated from magnetopause conditions in Figure 1. Hence, we can assume a sufficiently thin magnetopause current sheet irrespective of Ganymede's position relative to the Jovian current sheet.

The remaining two onset conditions effectively limit local plasma flows to be below the characteristic Alfvén speed associated with reconnection, with suppression of reconnection above this limit. The second onset condition concerns the diamagnetic drift between plasma electrons and ions within the magnetopause current sheet, leading to a condition involving the magnetic shear angle

$$\theta_{sh} > 2tan^{-1}\left(\frac{d_i \Delta\beta}{L}\right) = 2tan^{-1}(\Delta\beta),$$

where θ_{sh} is the smaller shear angle between the Jovian and Ganymedean magnetic fields in a magnetopause-tangent plane at each grid point (Swisdak et al., 2003, 2010). If this condition is unsatisfied, the diamagnetic drift is too fast and reconnection is suppressed. The system length scale (L) is the
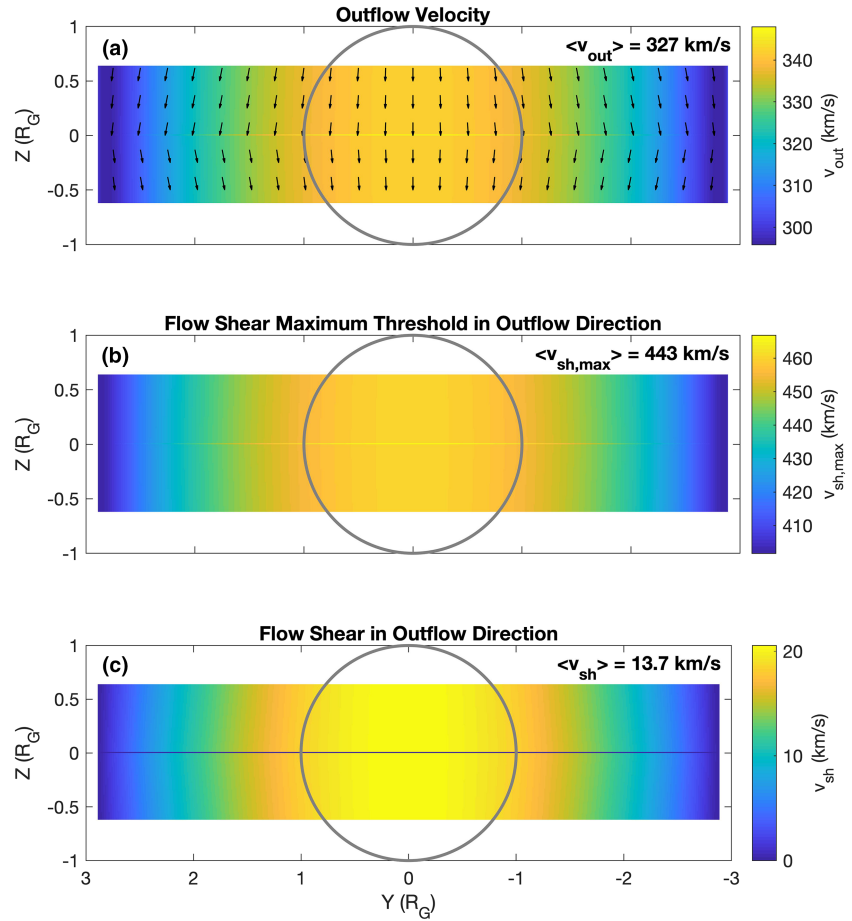
Figure 3. Evaluation of the bulk plasma flow shear onset condition in Ganymede's closed-field regions when Ganymede is in the Jovian current sheet. Parameters shown are (a) reconnection outflow velocity, (b) flow shear maximum threshold in outflow direction, and (c) flow shear in outflow direction calculated from magnetopause conditions. The format is the same as Figure 2.

magnetopause current sheet thickness, which from the first onset condition is approximately equal to the ion inertial length (d_i), so the shear angle minimum threshold depends only on the beta difference $(\beta = \beta_J - \beta_G)$ across the magnetopause. As Ganymede contributes negligible plasma pressure $(\beta_G = 0)$, $\Delta\beta$ is equal to the Jovian-side beta $\beta_J = P_{J,p}/P_{J,b}$. The third onset condition concerns the flow shear between Jovian and Ganymedean bulk plasmas adjacent to the magnetopause current sheet along the reconnection outflow direction. Each magnetopause location has two outflow vectors parallel/antiparallel to the cross product of the vector bisecting the smaller shear angle between Jovian and Ganymedean magnetic field lines and the local magnetopause-normal vector (Masters, 2017). We choose the southward pointing primary outflow vector following the Jovian field lines and define the flow shear condition:

$$v_{sh} = \frac{|v_1 - v_2|}{2} < v_{out}\left(\frac{\rho_1 B_2 + \rho_2 B_1}{2(\rho_1 B_2 \rho_2 B_1)^{1/2}}\right),$$

$$v_{out} = \left(\frac{B_1 B_2 (B_1 + B_2)}{\mu_0(\rho_1 B_2 + \rho_2 B_1)}\right)^{1/2},$$

where symbol definitions are v = flow velocity, ρ = mass density, B = magnetic field strength, and $\mu_0 = 4\pi \times 10^{-7}$ H/m (Doss et al., 2015). Subscripts 1 and 2 indicate parameter projections along the outflow vector on Jovian side and Ganymedean side, respectively. The flow shear is v_{sh} and the outflow speed is v_{out}. Reconnection is suppressed if the flow shear exceeds its maximum threshold.

We first assess these two onset conditions for a specific case when Ganymede is in the Jovian current sheet and then consider two extreme cases when Ganymede is furthest above/below the current sheet. Figure 2 assesses the diamagnetic drift condition when Ganymede is in the current sheet. Beta differences in Figure 2a have the average of 2.02 in the closed-field region, with largest $\Delta\beta$ along the magnetopause flanks where the Jovian-side magnetic field is weakest. The resulting shear angle minimum thresholds ($\theta_{sh,min}$) in Figure 2b have the average of 90.3° with largest values along the flanks. Figure 2c shows magnetic shear angles calculated using data from Figures 1e and 1f. The average θ_{sh} is 175° with largest values in columns nearest to the subflow point and toward the flanks. Comparing Figures 2b and 2c indicates that $\theta_{sh} > \theta_{sh,min}$ at every point in the closed-field region, satisfying the second onset condition everywhere on Ganymede's magnetopause.

Figure 3 assesses the flow shear condition when Ganymede is in the current sheet. Reconnection outflow speeds in Figure 3a have the average of 327 km/s in the closed-field region with largest values along columns near the subflow point, where magnetic fields are most strongly aligned with outflow vectors. The resulting maximum flow shear thresholds ($v_{sh,max}$) in Figure 3b have the average of 443 km/s with largest values near the subflow point. Figure 3c shows flow shears calculated from the Jovian plasma flow in Figure 1d. The average v_{sh} is 13.7 km/s with largest values near the subflow point from outflow-aligned magnetic fields. Flow shears are also noticeably smaller along $Z = 0$ line where the Jovian plasma flow stagnates. Comparing Figures 3b and 3c indicates that $v_{sh} < v_{sh,max}$ at every point in the closed-field region, satisfying the third onset condition everywhere on Ganymede's magnetopause.

Consequently, magnetic reconnection can occur anywhere on Ganymede's magnetopause when Ganymede is in the current sheet. The electric field associated with reconnection follows (Doss et al., 2015)

$$E = 2k \left(\frac{B_1 B_2}{B_1 + B_2} \right) v_{out} \left(1 - \frac{(v_1 - v_2)^2}{(v_{out})^2} \frac{\rho_1 B_2 \rho_2 B_1}{(\rho_1 B_2 + \rho_2 B_1)^2} \right),$$

where the near-Earth reconnection efficiency factor $k = 0.1$ is adopted as it has no known β dependence (e.g., Masters, 2017; Paschmann et al., 2013). Figure 4a shows the electric field when Ganymede is in the current sheet with average magnitude 3.2 mV/m. Strongest field magnitudes are found along near-subflow columns corresponding to largest outflow speed locations. We also track (following Cooling et al., 2001) parcels of plasma in reconnection outflows from three equatorial reconnection sites—one at the subflow point and two others at midflanks ($Y = \pm 1.5\ R_G$). All outflows travel bidirectionally north/south away from Ganymede's equator. However, the subflow site's outflows remain on the magnetopause symmetry plane ($Z = 0$) while the midflank sites' outflows shift toward their nearest flanks due to influence from the Jovian-side plasma flow.

Figures 4b and 4c, respectively, show reconnection assessment when Ganymede is furthest above and below the current sheet, with magnetopause asymmetries and ambient parameters adjusted accordingly. Despite condition changes, the electric fields remain nonzero throughout closed-field regions, so reconnection is also possible anywhere on the magnetopause when Ganymede is furthest above/below the current sheet. The electric field varies symmetrically north/south of the current sheet and becomes stronger along the flanks where Jupiter's and Ganymede's magnetic fields are now most strongly antiparallel. The average electric field also increases from 3.2 to 5.1 mV/m at extreme Ganymede positions. Small discontinuities are observed across lines containing the subflow point, reflecting sharp turns on the magnetopause arising from the surface equations. A more realistic magnetopause surface would be smoother, and so the discontinuities should disappear.

4. Discussion

Since there appears to be no restrictions for reconnection onset when Ganymede's magnetopause is symmetric and most asymmetric, we can generalize that reconnection is favorable anywhere on the magnetopause for all magnetopause asymmetries, that is, all positions along Ganymede's orbit of Jupiter. This result is consistent with widespread reconnection events observed in global simulations (e.g., Jia, Walker, et al., 2010; Tóth et al., 2016)
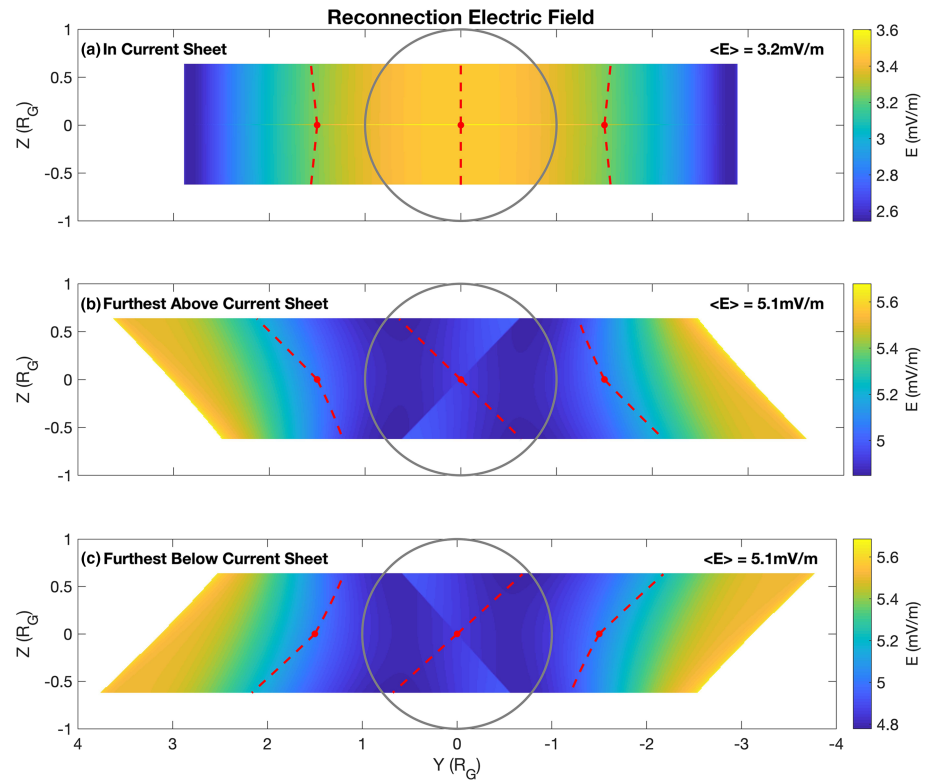
Figure 4. Electric field at potential reconnection sites in Ganymede's closed-field regions computed when Ganymede is (a) in, (b) furthest above, and (c) furthest below the Jovian current sheet. Red dashed lines indicate plasma outflow tracks from selected reconnection sites. The format is the same as Figure 2.

The electric field magnitude range (2.6 – 5.6 mV/m) modeled is much larger compared to those at Earth's (<0.01 – 0.2 mV/m) and Jupiter's (<0.1 mV/m) magnetopauses (Masters, 2017; Paschmann et al., 2013), indicating significant reconnection rates at all Ganymedean magnetopause locations. Although a dominant X line is possible, this electric field configuration highlights possibilities for less ordered reconnection site distributions, such as multiple large X lines or widespread transient flux-transfer events (seen in global simulations), at Ganymede's magnetopause.

The electric field equation is found most sensitive to changes in magnetic parameters B_1 and B_2. As Ganymede moves further away from the Jovian current sheet, the ambient Jovian magnetic field becomes stronger, increasing both B_1 and B_2 (the latter due to the model's fixed magnetopause surface). The average electric field increases in Figure 4 are therefore dependent on Ganymede's position and controlled by Jupiter's east longitude ϕ. As the Jovian dipole rotates rapidly, each ϕ value also corresponds to a distinct time of day on Jupiter. Hence magnetic reconnection rate at Ganymede exhibits a Jovian-diurnal variation and is effectively driven by Jupiter's rotation. The conclusion has been independently supported by remote observations of Jovian radio emissions associated with Ganymede (Zarka et al., 2018).

Multiplying the average electric fields by the magnetopause width (~6 R_G) gives 50–80 kV reconnection voltage estimates at Ganymede's magnetopause, which may be used to constrain reconnection rate in the magnetotail via open magnetic flux conservation. We also calculate reconnection-induced electron and ion temperature increases of 250–560 eV and 2,000–4,200 eV, respectively, using empirical methods from Earth-based studies (Phan et al., 2013, 2014), with the maximum (minimum) value corresponding to when Ganymede is furthest above/below (in) the Jovian current sheet. These numbers far exceed ambient temperatures for electrons and ions of 300 and 60 eV, respectively (Kivelson et al., 2004); hence, reconnection should result in particle heating signatures observable by the upcoming JUICE mission.

5. Summary

Ganymede's permanent magnetic field and its resulting magnetosphere present a unique opportunity to study magnetic reconnection in a sub-Alfvénic plasma flow environment. We present an analytical model of steady-state conditions at Ganymede's upstream magnetopause, from which we conduct the first assessment of reconnection onset theory at this boundary. The model shows that reconnection may occur anywhere on the magnetopause where Ganymede's closed magnetic field encounters Jupiter's ambient field, and the onset appears largely unaffected by Ganymede's position relative to the Jovian current sheet. This result is consistent with previous global MHD simulations of Ganymede's magnetosphere and highlights possibilities for less orderly reconnection structures (multiple X lines and widespread flux-transfer events) at Ganymede's magnetopause.

The average reconnection rate is shown to be a function of Ganymede's position along its orbit around Jupiter, which approximately corresponds to the time of day on Jupiter. Hence, the reconnection rate exhibits a Jovian-diurnal variation and is effectively driven by Jupiter's rotation. The reconnection process should heat up surrounding plasma particles producing signatures detectable by spacecraft instruments. Our steady-state model currently does not capture orientation changes of Ganymede's magnetic field due to the moon's subsurface ocean. Future integration of ocean effects will allow more accurate predictions of reconnection structures in preparation for the JUICE space mission.

References

Alexeev, I. I., Sibeck, D. G., & Bobrovnikov, S. Y. (1998). Concerning the location of magnetopause merging as a function of the magnetopause current strength. *Journal of Geophysical Research*, *103*(A4), 6675–6684. https://doi.org/10.1029/97JA02863

Anderson, J. D., Lau, E. L., Sjogren, W. L., Schubert, G., & Moore, W. B. (1996). Gravitational constraints on the internal structure of Ganymede. *Nature*, *384*(6609), 541–543. https://doi.org/10.1038/384541a0

Bills, B. G. (2005). Free and forced obliquities of the Galilean satellites of Jupiter. *Icarus*, *175*(1), 233–247. https://doi.org/10.1016/j.icarus.2004.10.028

Cooling, B. M. A., Owen, C. J., & Schwartz, S. J. (2001). Role of the magnetosheath flow in determining the motion of open flux tubes. *Journal of Geophysical Research*, *106*(A9), 18,763–18,775. https://doi.org/10.1029/2000JA000455

Cowley, S. W. H., Bunce, E. J., & Nichols, J. D. (2003). Origins of Jupiter's main oval auroral emissions. *Journal of Geophysical Research*, *108*(A4), 8002. https://doi.org/10.1029/2002ja009329

Daldorff, L. K. S., Tóth, G., Gombosi, T. I., Lapenta, G., Amaya, J., Markidis, S., & Brackbill, J. U. (2014). Two-way coupling of a global Hall magnetohydrodynamics model with a local implicit particle-in-cell model. *Journal of Computational Physics*, *268*, 236–254. https://doi.org/10.1016/j.jcp.2014.03.009

Desroche, M., Bagenal, F., Delamere, P. A., & Erkaev, N. (2012). Conditions at the expanded Jovian magnetopause and implications for the solar wind interaction. *Journal of Geophysical Research*, *117*, A07202. https://doi.org/10.1029/2012JA017621

Desroche, M., Bagenal, F., Delamere, P. A., & Erkaev, N. (2013). Conditions at the magnetopause of Saturn and implications for the solar wind interaction. *Journal of Geophysical Research: Space Physics*, *118*, 3087–3095. https://doi.org/10.1002/jgra.50294

Dorelli, J. C., Glocer, A., Collinson, G., & Tóth, G. (2015). The role of the Hall effect in the global structure and dynamics of planetary magnetospheres: Ganymede as a case study: Hall reconnection at Ganymede. *Journal of Geophysical Research*: Space Physics, *120*, 5377–5392. https://doi.org/10.1002/2014JA020951

Doss, C. E., Komar, C. M., Cassak, P. A., Wilder, F. D., Eriksson, S., & Drake, J. F. (2015). Asymmetric magnetic reconnection with a flow shear and applications to the magnetopause. *Journal of Geophysical Research: Space Physics*, *120*, 7748–7763. https://doi.org/10.1002/2015JA021489

Frank, L. A., Paterson, W. R., Ackerson, K. L., & Bolton, S. J. (1997). Outflow of hydrogen ions from Ganymede. *Geophysical Research Letters*, *24*(17), 2151–2154. https://doi.org/10.1029/97GL01744

Grasset, O., Dougherty, M. K., Coustenis, A., Bunce, E., Erd, C., Titov, D. V., et al. (2013). JUpiter ICy moons Explorer (JUICE): An ESA mission to orbit Ganymede and to characterise the Jupiter system. *Planetary and Space Science*, *78*, 1–21. https://doi.org/10.1016/j.pss.2012.12.002

Gurnett, D. A., Kurth, W. S., Roux, A., Bolton, S. J., & Kennel, C. F. (1996). Evidence for a magnetosphere at Ganymede from plasma-wave observations by the Galileo spacecraft. *Nature*, *384*(6609), 535–537. https://doi.org/10.1038/384535a0

Jia, X., Kivelson, M. G., Khurana, K. K., & Walker, R. J. (2010). Magnetic fields of the satellites of Jupiter and Saturn. *Space Science Reviews*, *152*(1-4), 271–305. https://doi.org/10.1007/s11214-009-9507-8

Jia, X., Walker, R. J., Kivelson, M. G., Khurana, K. K., & Linker, J. A. (2008). Three-dimensional MHD simulations of Ganymede's magnetosphere. *Journal of Geophysical Research*, *113*, A06212. https://doi.org/10.1029/2007JA012748

Jia, X., Walker, R. J., Kivelson, M. G., Khurana, K. K., & Linker, J. A. (2009). Properties of Ganymede's magnetosphere inferred from improved three-dimensional MHD simulations. *Journal of Geophysical Research: Space Physics*, *114*, A09209. https://doi.org/10.1029/2009JA014375

Jia, X., Walker, R. J., Kivelson, M. G., Khurana, K. K., & Linker, J. A. (2010). Dynamics of Ganymede's magnetopause: Intermittent reconnection under steady external conditions. *Journal of Geophysical Research*, *115*, A12202. https://doi.org/10.1029/2010JA015771

Kaweeyanun, N. (2020). Favorable conditions for magnetic reconnection at Ganymede's upstream magnetopause. Version 1.0. Imperial College High Performance Computing Service Data Repository. https://doi.org/10.14469/hpc/6738. .

Khurana, K. K. (1997). Euler potential models of Jupiter's magnetospheric field. *Journal of Geophysical Research*, *102*(A6), 11,295–11,306. https://doi.org/10.1029/97JA00563

Kivelson, M. G., Bagenal, F., Kurth, W. S., Neubauer, F. M., Paranicas, C., & Saur, J. (2004). Magnetospheric interactions with satellites. In F. Bagenal (Ed.), *Jupiter. The Planet, Satellites and Magnetosphere* (Vol. 1, pp. 513–536). Cambridge, U.K.: Cambridge University Press. ISBN 0-521-81808-7.

Kivelson, M. G., Khurana, K. K., Coroniti, F. V., Joy, S., Russell, C. T., Walker, R. J., et al. (1997). The magnetic field and magnetosphere of Ganymede. *Geophysical Research Letters*, *24*(17), 2155–2158. https://doi.org/10.1029/97GL02201

Kivelson, M. G., Khurana, K. K., Russell, C. T., Walker, R. J., Warnecke, J., Coroniti, F. V., et al. (1996). Discovery of Ganymede's magnetic field by the Galileo spacecraft. *Nature*, *384*(6609), 537–541. https://doi.org/10.1038/384537a0

Kivelson, M. G., Khurana, K. K., & Volwerk, M. (2002). The permanent and inductive magnetic moments of Ganymede. *Icarus*, *157*(2), 507–522. https://doi.org/10.1006/icar.2002.6834

Kivelson, M. G., Warnecke, J., Bennett, L., Joy, S., Khurana, K. K., Linker, J. A., et al. (1998). Ganymede's magnetosphere: Magnetometer overview. *Journal of Geophysical Research*, *103*(E9), 19,963–19,972. https://doi.org/10.1029/98JE00227

Leclercq, L., Modolo, R., Leblanc, F., Hess, S., & Mancini, M. (2016). 3D magnetospheric parallel hybrid multi-grid method applied to planet–plasma interactions. *Journal of Computational Physics*, *309*, 295–313. https://doi.org/10.1016/j.jcp.2016.01.005

Masters, A. (2014). Magnetic reconnection at Uranus' magnetopause. *Journal of Geophysical Research: Space Physics*, *119*, 5520–5538. https://doi.org/10.1002/2014JA020077

Masters, A. (2015a). The dayside reconnection voltage applied to Saturn's magnetosphere. *Geophysical Research Letters*, *42*, 2577–2585. https://doi.org/10.1002/2015GL063361

Masters, A. (2015b). Magnetic reconnection at Neptune's magnetopause. *Journal of Geophysical Research: Space Physics*, *120*, 479–493. https://doi.org/10.1002/2014JA020744

Masters, A. (2017). Model-based assessments of magnetic reconnection and Kelvin-Helmholtz instability at Jupiter's magnetopause. *Journal of Geophysical Research: Space Physics*, *122*, 11,154–11,174. https://doi.org/10.1002/2017JA024736

McKinnon, W. B. (1997). Galileo at Jupiter—Meetings with remarkable moons. *Nature*, *390*(6655), 23–26. https://doi.org/10.1038/36222

Neubauer, F. M. (1998). The sub-Alfvenic interaction of the Galilean satellites with the Jovian magnetosphere *Journal of Geophysical Research*, *103*(E9), 19,843–19,866

Neubauer, F. M. (1990). Satellite plasma interactions. *Advances in Space Research*, *10*(1), 25–38. https://doi.org/10.1016/0273-1177(90)90083-C

Paschmann, G., Øieroset, M., & Phan, T. (2013). In-situ observations of reconnection in space. *Space Science Reviews*, *178*(2-4), 385–417. https://doi.org/10.1007/s11214-012-9957-2

Petrinec, S. M., & Russell, C. T. (1997). Hydrodynamic and MHD equations across the bow shock and along the surface of planetary obstacles. *Space Science Reviews*, *79*(3/4), 757–791. https://doi.org/10.1023/A:1004938724300

Phan, T. D., Drake, J. F., Shay, M. A., Gosling, J. T., Paschmann, G., Eastwood, J. P., et al. (2014). Ion bulk heating in magnetic reconnection exhausts at Earth's magnetopause: Dependence on the inflow Alfvén speed and magnetic shear angle. *Geophysical Research Letters*, *41*, 7002–7010. https://doi.org/10.1002/2014GL061547

Phan, T. D., Love, T. E., Gosling, J. T., Paschmann, G., Eastwood, J. P., Oieroset, M., et al. (2011). Triggering of magnetic reconnection in a magnetosheath current sheet due to compression against the magnetopause. *Geophysical Research Letters*, *38*, L17101. https://doi.org/10.1029/2011GL048586

Phan, T. D., Shay, M. A., Gosling, J. T., Fujimoto, M., Drake, J. F., Paschmann, G., et al. (2013). Electron bulk heating in magnetic reconnection at Earth's magnetopause: Dependence on the inflow Alfvén speed and magnetic shear. *Geophysical Research Letters*, *40*(17), 4475–4480. https://doi.org/10.1002/grl.50917

Schubert, G., Zhang, K., Kivelson, M. G., & Anderson, J. D. (1996). The magnetic field and internal structure of Ganymede. *Nature*, *384*(6609), 544–545. https://doi.org/10.1038/384544a0

Swisdak, M., Opher, M., Drake, J. F., & Alouani Bibi, F. (2010). The vector direction of the. *Interstellar Magnetic Field Outside the Heliosphere.*, *710*(2), 1769–1775. https://doi.org/10.1088/0004-637x/710/2/1769

Swisdak, M., Rogers, B., Drake, J. F., & Shay, M. (2003). Diamagnetic suppression of component magnetic reconnection at the magnetopause. *Journal of Geophysical Research*, *108*(A5), 1218. https://doi.org/10.1029/2002JA009726

Tóth, G., Jia, X., Markidis, S., Peng, I. B., Chen, Y., Daldorff, L. K. S., et al. (2016). Extended magnetohydrodynamics with embedded particle-in-cell simulation of Ganymede's magnetosphere. *Journal of Geophysical Research: Space Physics*, *121*, 1273–1293. https://doi.org/10.1002/2015JA021997

Trattner, K. J., Mulcock, J. S., Petrinec, S. M., & Fuselier, S. A. (2007a). Location of the reconnection line at the magnetopause during southward IMF conditions. *Geophysical Research Letters*, *34*(3), L03108. https://doi.org/10.1029/2006GL028397

Trattner, K. J., Mulcock, J. S., Petrinec, S. M., & Fuselier, S. A. (2007b). Probing the boundary between antiparallel and component reconnection during southward interplanetary magnetic field conditions. *Journal of Geophysical Research*, *112*, n/a. https://doi.org/10.1029/2007JA012270

Williams, D. J., Mauk, B., & McEntire, R. W. (1997). Trapped electrons in Ganymede's magnetic field. *Geophysical Research Letters*, *24*(23), 2953–2956. https://doi.org/10.1029/97GL03003

Williams, D. J., Mauk, B. H., McEntire, R. W., Roelof, E. C., Armstrong, T. P., Wilken, B., et al. (1997). Energetic particle signatures at Ganymede: Implications for Ganymede's magnetic field. *Geophysical Research Letters*, *24*(17), 2163–2166. https://doi.org/10.1029/97GL01931

Zarka, P., Soares Marques, M., Louis, C., Ryabov, V., Lamy, L., Echer, E., & Cecconi, B. (2018). Jupiter radio emission induced by Ganymede and consequences for the radio detection of exoplanets. *Astronomy and Astrophysics*, *618*, A84. https://doi.org/10.1051/0004-6361/201833586

Zhou, H., Tóth, G., Jia, X., Chen, Y., & Markidis, S. (2019). Embedded kinetic simulation of Ganymede's magnetosphere: Improvements and inferences. *Journal of Geophysical Research: Space Physics*, *124*(7), 5441–5460. https://doi.org/10.1029/2019JA026643